Electronic structure of two-dimensional magnetic alloys: $c(2\times2)$ Mn on Cu(100) and Ni(100)

O. Rader* and W. Gudat
BESSY, Lentzeallee 100, D-14195 Berlin, Germany

C. Carbone, E. Vescovo,† S. Blügel, R. Kläsges, and W. Eberhardt
Institut für Festkörperforschung, Forschungszentrum Jülich, D-52425 Jülich, Germany

M. Wuttig
Institut für Grenzflächenforschung und Vakuumphysik, Forschungszentrum Jülich, D-52425 Jülich, Germany

J. Redinger
Institut für Technische Elektrochemie, Technische Universität Wien, Getreidemarkt 9/158, A-1060 Wien, Austria

F. J. Himpsel‡
IBM Thomas J. Watson Research Center, P.O. Box 218, Yorktown Heights, New York 10598
(Received 5 June 1995; revised manuscript received 3 October 1996)

Half a monolayer (ML) of Mn deposited above 270 K on the (100) surfaces of Cu and Ni form ordered surface alloys of $c(2\times2)$ structure. Their electronic structure is studied in a combined experimental and theoretical work. The experimental approach, comprising angle-resolved photoemission and inverse photoemission, characterizes both systems as ideal cases of well-ordered magnetic surface alloys. A large atomiclike splitting between majority- and minority-spin Mn-3d states is measured: 5.5 eV for the Cu-based system and 5.25 eV for the Ni-based system. The large splittings are direct evidence that Mn develops a high local magnetic moment in these systems. Our first-principles band-structure calculations of $c(2\times2)$ CuMn/Cu(100) and $c(2\times2)$ NiMn/Ni(100) corroborate this finding and give values of $3.75\mu_B$ and $3.5\mu_B$, respectively, for the Mn moments. We find that the measured splittings are even larger than the ones calculated from first principles. The difference amounts to 2.7 eV and 1.7 eV for the Cu-based and Ni-based system, respectively. We suppose that the splitting measured in photoemission and inverse photoemission is increased by a Coulomb energy U due to the enhanced localization of the Mn-3d states in the surface alloy. This high localization can be quantified by the small band dispersion of 110 ± 60 meV measured for the Mn minority d band in the Cu-based system. We also investigated the work-function change upon surface-alloy formation. By comparing our results with our *ab initio* calculations we identified the magnetism as the source of the work-function change. [S0163-1829(97)02908-1]

I. INTRODUCTION

The systems $c(2\times2)$ CuMn/Cu(100) and $c(2\times2)$ NiMn/Ni(100) represent a recently discovered class of materials, i.e., ordered two-dimensional magnetic alloys.[1–4] They consist of a 1-ML-thick alloy film of CuMn (NiMn), with a checkerboard structure of Mn and Cu (Ni) sites. In this paper we characterize the electronic structure of both alloys in an approach combining photoelectron spectroscopy for occupied electronic states and inverse photoemission for unoccupied states with local-density band-structure calculations from first principles in order to decide which aspects are dominating the electronic properties of these new surface alloys.

One important aspect for the electronic structure of these systems is the geometrical structure of an ordered surface alloy. The same $c(2\times2)$ superstructure is also realized for two other surface alloys stabilized on Cu(100), namely $c(2\times2)$ CuAu/Cu(100) (Ref. 5) and $c(2\times2)$ CuPd/Cu(100),[6] but the surface alloys discussed here show some unusual properties: One is that the ordered-surface-alloy structure $c(2\times2)$ CuMn/Cu(100) forms although there exists no ordered bulk CuMn phase. Usually it is the other way around insofar as ordered bulk alloys often show disorder at the surface due to surface segregation. Second, low-energy electron diffraction (LEED) measurements showed that the Mn atoms exhibit an unusually large outward relaxation of 0.25 ±0.02 Å (14.2%) in $c(2\times2)$ NiMn/Ni(100) (Ref. 3) and 0.30 ±0.02 Å (16.6%) in $c(2\times2)$ CuMn/Cu(100).[2] For comparison, the surface atom buckling of the $c(2\times2)$ CuAu/Cu(100) is less than 6% (Ref. 5) although the atomic radius of Au is larger than that of Mn. There are strong indications that the magnetism of the surface alloys is the origin of these unusual properties. These indications are based on the impact of magnetism on the structure and stability of the surface alloys and come from *ab initio* electronic-structure calculations. Structural optimizations performed for the CuMn and NiMn surface-alloy systems showed that (i) the alloys are magnetic with large Mn moments of $3.75\mu_B$ for the $c(2\times2)$ CuMn/Cu(100) alloy and $3.5\mu_B$ for the $c(2\times2)$ NiMn/Ni(100) alloy, (ii) only magnetism gives rise to the outward relaxation,[2] and (iii) the large magnetic moment of Mn is the basic source for the formation and the stability[2] of the surface alloys.[7] The line shape of soft x-ray absorption spectra of

$c(2\times2)$ CuMn/Cu(100) and $c(2\times2)$ NiMn/Ni(100) was found to be in agreement with large Mn magnetic moments.[8,9] The system $c(2\times2)$ NiMn/Ni(100) was very recently studied by magnetic circular x-ray dichroism.[9,10] This system is best described as a semi-infinite magnet with a NiMn monolayer in the external field provided by the Ni substrate, and ferromagnetic order of the Mn moments and ferromagnetic coupling to the Ni substrate was found.[9,10]

The second interesting aspect determining the electronic structure is therefore magnetism, and the Mn $c(2\times2)$ surface alloys can be considered a special case of magnetic monolayers on the noble metal Cu. Transition-metal monolayers on noble metals have been investigated experimentally in the past years and are successfully described by local-density band theory. Their key property and main reason for the experimental and theoretical interest is their enhanced magnetism. The itinerant magnetism of transition metals depends strongly on the dimensionality of the system, or, strictly speaking, on the coordination number of the transition-metal atoms in these systems. The magnetism of single atoms, for example, is governed by Hund's rule, and the electron spins are aligned parallel as long as the double occupancy of a quantum number is not violated. This leads for a Mn atom to the largest possible d moment in the $3d$ series of $5\mu_B$. For bulk metals the magnetic moments are in most cases absent because of the d-d hybridization to neighboring atoms, and only few transition metals (Cr,Mn,Fe,Co,Ni) remain magnetic. Transition metals in two dimensions should behave between these two extremes, and therefore materials near the middle of the transition-metal series are, in general, promising candidates for the achievement of maximum magnetic moments in the monolayer. Both Mn and Cr have shown strongly enhanced magnetic exchange splittings as monolayers on Ag(100) and Au(100).[11,12] Where majority-spin and minority-spin states were accessible in the experiment, a sufficient description of the enhanced splitting is given by theory: For an Fe monolayer on Au(100) the exchange splitting from spin-resolved photoemission and inverse photoemission, 2.7 eV (Refs. 13 and 14) compares reasonably well with the theoretical prediction for the same pair of states, 2.4 eV.[15] For a Cr monolayer on Ag(100) the splitting found from photoemission and inverse photoemission is 2.7 eV,[11,12,16] the theoretical one about 3.3 eV.[17] The measured and predicted splittings for monolayers are significantly larger than the respective bulk values [1.8–2.1 eV for Fe,[18] 0.13 eV for Cr (Ref. 19)]. For $c(2\times2)$ CuMn/Cu(100) the theoretical expectation for the spin-split local density of states (LDOS) of Mn is displayed in Fig. 1(a). Compared to bulk Mn one sees an enhancement in the magnetic splitting and moment. The calculations assume a ferromagnetic ground-state configuration, and the majority-spin and minority-spin states are split by 2.7 eV. As we will show below, our experiments lead to a splitting of 5.5 eV, thus considerably larger than the theoretical value.

We can explain this property as a result of the combination of the two aspects mentioned above, i.e., firstly the surface-alloy geometry leading to a regular lattice of isolated Mn atoms and secondly the magnetism of Mn. We argue that the localization of the d states in nearly isolated Mn atoms has to be taken into account, which increases their exchange/

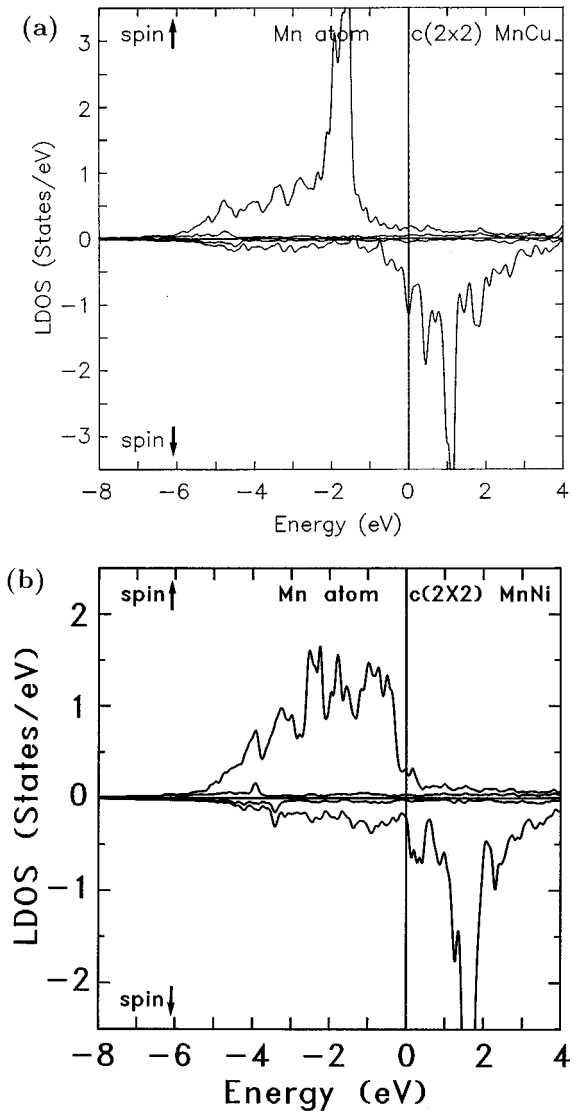

FIG. 1. Calculated spin-resolved local density of states (LDOS) at the Mn site for (a) $c(2\times2)$ CuMn/Cu(100) and (b) $c(2\times2)$ NiMn/Ni(100) showing the magnetic exchange splitting between minority (negative LDOS) and majority spin (positive LDOS) states.

Coulomb splitting. Although the hybridization of d states is expected to be stronger among Mn and Ni than among Mn and Cu [this can, e.g., be seen from the broader majority-spin density of states in Fig. 1(b) as compared to Fig. 1(a)], we find a similar situation for Mn in $c(2\times2)$ NiMn/Ni(100).

A good reference point for the localization of Mn-$3d$ states are dilute Mn atoms in noble metals where the enhancement of the magnetic splitting and moment is even larger than in monolayers on noble metals. In such systems large moments have been measured: For Mn impurities in Cu $3.54\pm0.10\mu_B$ were measured by neutron scattering at 4.2 K;[20] $3.4\mu_B$ was obtained from an analysis of de Haas–van Alphen experiments.[21] For Mn impurities in Ni neutron scattering gives $3.50\mu_B$ at 4.2 K and $2.63\mu_B$ at room temperature.[22] Recently, Mn impurities in Ni were also studied by magnetic circular x-ray dichroism, and $2.25\pm0.35\mu_B$ was obtained at room temperature.[23]

II. THEORETICAL METHODS

We have conducted *ab initio* electronic-structure calculations. These calculations are based on the density-functional theory in the local-spin-density approximation.[24] The equations are solved using the full-potential linearized-augmented plane-wave method for thin-film geometry.[25] Self-consistent calculations of the $c(2\times2)$ CuMn/Cu(100) system were performed for a seven-layer film consisting of five layers of Cu with 2 Cu atoms per layer representing the $c(2\times2)$ Cu(100) substrate and on top of each Cu surface one Mn and one Cu atom arranged in a checkerboard structure simulating the $c(2\times2)$ surface alloy. The positions of the Mn and Cu surface-alloy atoms with respect to the substrate atoms were obtained from the structural optimization by total-energy minimization.[2,26] For $c(2\times2)$ NiMn/Ni(100) essentially the same arrangement was used. Here, seven Ni layers were used adding up to a total thickness of a nine-layer slab to model the $c(2\times2)$ NiMn/Ni(100) surface alloy. A structure optimization was also performed for this system.[26] The local densities of states of Mn in $c(2\times2)$ CuMn/Cu(100) and $c(2\times2)$ NiMn/Ni(100) are shown in Fig. 1. The magnetic moments of the Mn surface alloy atoms on the Cu(100) substrate were determined to $3.75\mu_B$ and to $3.5\mu_B$ on the Ni(100) substrate. While the film thickness used so far is sufficient to provide converged results on the layer dependent potentials and integrated quantities such as the magnetic moments, this film thickness makes it difficult to distinguish the states which belong to the bulk-projected bands of the substrate, the bulk band gaps and the Mn-derived states. Therefore, the band structures shown below originate from thick films of 19 layers for the Cu-based system and 21 layers for the Ni-based system. We find that the substrate bands of these films clearly approach the continuous spectrum of states of the projected-bulk bands describing the semi-infinite substrate. The potentials and densities for these thick films were taken from the thinner films applying a stretching technique.[27] In addition, we carried out self-consistent calculations of Cu(100) and Ni(100) surfaces in order to determine the work-function change due to alloying and magnetism.

III. EXPERIMENTAL SETUP AND SAMPLE PREPARATION

In this study two different experimental setups were used for (i) inverse photoemission and (ii) spin- and angle-resolved photoemission. (i) The inverse photoemission experiments were performed at the IBM Thomas J. Watson Research Center with the spectrograph described in Ref. 28. The polarization geometry was such that for normal-incident electrons the electric-field vector parallel to the surface was weighted three times as much as the perpendicular component. This emphasizes states with $d_{xz,yz}$ symmetry as opposed to those with d_{z^2} symmetry. (ii) The angle-resolved photoemission experiments were performed at the BESSY synchrotron light source with the spectrometer described in Ref. 29. Linearly polarized light from the TGM 1 beamline[30] was used to excite photoelectrons. In normal electron-emission geometry two light-polarization conditions were used: One in which the electric-field vector was entirely in the surface plane, basically used for the CuMn surface alloy [Figs. 2(a), 5(a), and 6(a)], and one with both parallel and perpendicular components, used for the NiMn surface alloy [Fig. 3(a)], with the component parallel to the surface larger by a factor of 1.7. The first geometry selects the $d_{xz,yz}$ states, the second a mixture of $d_{xz,yz}$ and d_{z^2}.

The Cu(100) and Ni(100) crystal surfaces were electropolished and prepared *in situ* by cycles of Ar sputtering and annealing at 700–1000 K. This procedure yielded sharp (1×1) LEED patterns and contaminant-free Auger electron spectra. The base pressure was 2×10^{-10} mbar in the photoemission chamber and 1×10^{-10} mbar in the inverse photoemission chamber. Mn was evaporated by means of electron bombardment from 99.98% pure pieces. A water-cooled jacket was used to reduce outgassing of the vacuum chamber. The Mn oven was repeatedly calibrated by an oscillating quartz thickness monitor on the basis of lattice constant and density of bulk α-Mn. Outgassing of the oven was conducted until Mn could be evaporated in the 10^{-10} mbar pressure range at a rate of typically 0.3 ML per min.

The $c(2\times2)$ CuMn/Cu(100) and $c(2\times2)$ NiMn/Ni(100) surface alloys were prepared according to the recipes given by Wuttig *et al.* [CuMn;[1,2,4] NiMn (Refs. 3 and 4)] by evaporation of nominally 0.5 ML Mn onto the Cu sample held at ambient temperature and onto the Ni sample held at about 450 K. Postannealing the $c(2\times2)$ NiMn/Ni(100) was occasionally found to improve the $c(2\times2)$ LEED pattern.

In the photoemission experiment a thick (25 ML) epitaxial Ni film on Cu(100) was prepared as substrate. The epitaxial growth of thinner (6 ML) Ni on Cu(100) by annealing after the Ni deposition and its stability against the heating were reported in Ref. 31. We grew thick Ni layers on Cu(100) in two steps with annealing to about 550 K after the first 10 ML and after completion of the film. The Ni thickness was such that no Cu-3d signal was observed in photoemission before and after the annealing. During and after the subsequent Mn deposition the sample was heated less than the Ni film before to ensure that no Cu interdiffusion would obscure the NiMn spectra.

The presence of a sharp and intense $c(2\times2)$ LEED pattern was verified prior to each photoemission measurement of the alloys with the exception of the photoemission experiment where the $c(2\times2)$ NiMn was grown on Ni/Cu(100). Here the superstructure was less sharp and less intense.

Moreover, we used a 100 keV Mott-type spin detector[29] attached to our photoemission setup in order to probe whether long-range ferromagnetic order exists in $c(2\times2)$ CuMn/Cu(100) at liquid-nitrogen temperature. The spin-detector geometry is sensitive to a sample magnetization lying in the surface plane, but no long-range ferromagnetic order was found at liquid-nitrogen temperature. For $c(2\times2)$ NiMn/Ni(100), for which ferromagnetic alignment of Mn moments has already been confirmed,[9] we did not perform spin analysis of the photoelectrons. The reason is that sufficiently thick films (here 25 ML) of Ni on Cu(100) had to be used in order to suppress Cu-3d emission in the spectra. However, for thicknesses larger than about 7 ML the magnetization lies in the [100] direction perpendicular to the surface,[32] to which our spin detector is not sensitive.

IV. MAJORITY AND MINORITY SPIN Mn 3*d* STATES

Photoemission and inverse photoemission spectra at zero parallel momentum are compared in Figs. 2(a) and 2(b) to

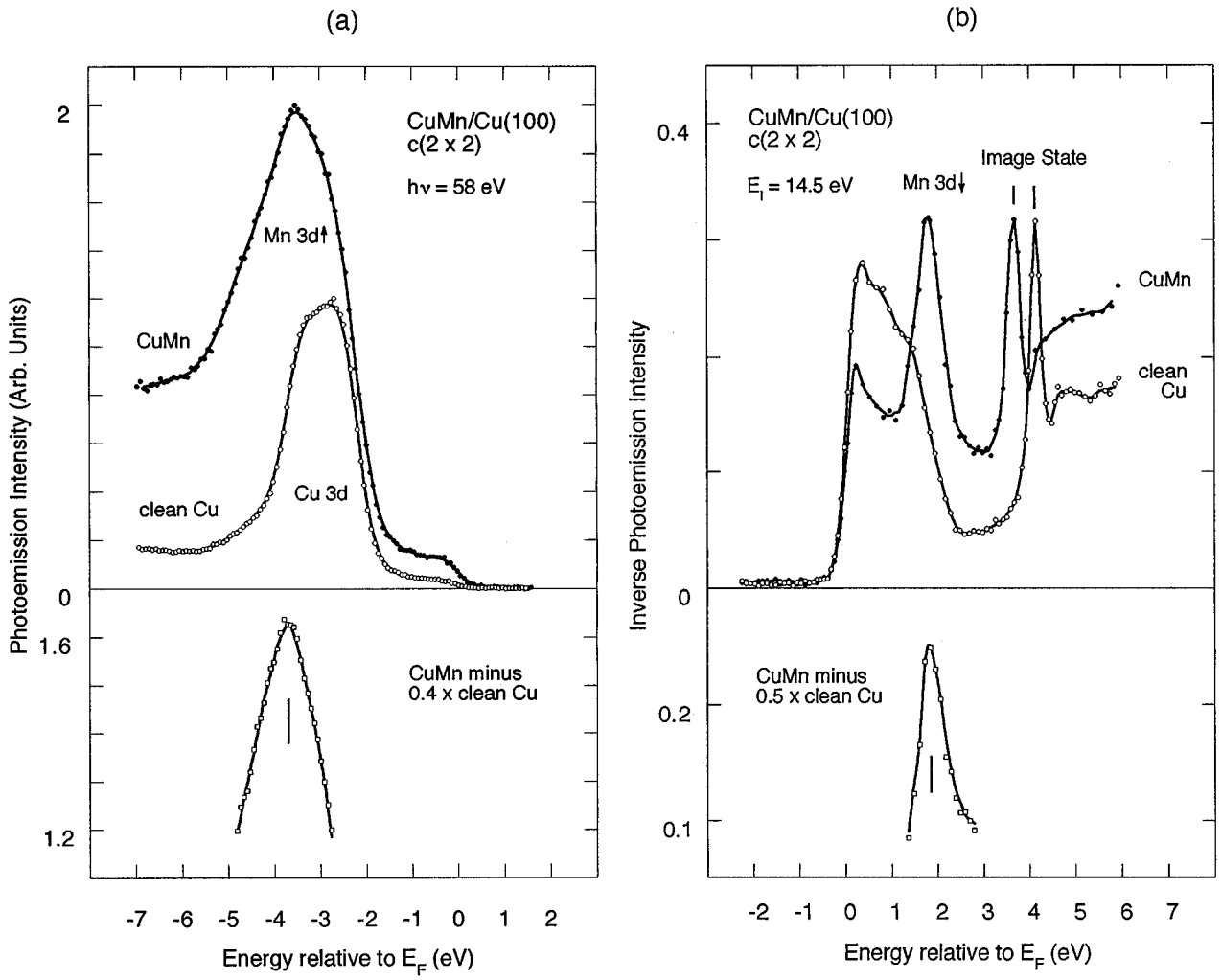

FIG. 2. Photoemission (a) and inverse photoemission (b) spectra for $c(2\times2)$ CuMn/Cu(100) at zero parallel momentum. The frames at the bottom show difference spectra after subtracting the substrate signal. Majority- and minority-spin Mn-3d states are seen at -3.7 eV and 1.85 eV. Image states in the inverse-photoemission spectra track the work function.

obtain the complete electronic structure of the $c(2\times2)$ CuMn/Cu(100). Figure 2(b) shows the inverse photoemission spectrum of $c(2\times2)$ CuMn/Cu(100) (filled circles) and clean Cu(100) (open circles). The Mn-3d states show up very clearly as a peak at 1.85 eV in inverse photoemission since there is no 3d background from the substrate. The shape of the spectrum between the 1.85-eV peak and the Fermi level appears unchanged with respect to that of the Cu substrate and is just attenuated by the Mn overlayer. Therefore, we conclude that the prevailing part of the Mn-3d emission is contained in the peak at 1.85 eV. This corraborates our theoretical prediction of a sharp minority-spin density of states far above the Fermi energy and thus an almost complete separation of unoccupied minority-spin states from occupied majority-spin states. The solitary Mn peak is therefore readily identified as minority spin. Its energy position can be compared to the result found for 0.2–1 ML of Mn on Ag(111) (Ref. 33). In that system Mn-3d emission is indeed found at a high energy of 1.8 eV,[33] however, accompanied by emission around 0.9 eV already at 0.2-ML coverage. For submonolayers Mn on Ag(100) (Ref. 11) a single peak was found, centered at 1.4 eV. In this case a broadening of the Mn-3d structure was observed for 1-ML nominal coverage and above.[11] The Mn-3d peak for $c(2\times2)$ CuMn/Cu(100) at 1.85 eV is very intense and sharper than its counterparts in complete 3d-metal monolayers and submonolayers on Ag(100), Au(100), and Cu(100).[11,12] The sharpness of this structure indicates the high crystalline order in the present system, which is confirmed by the image-state intensity (see below).

Cu s,p states form the weak background that is visible in Fig. 2(b) from the Fermi level to 1.8 eV above it, where a band gap in the Cu s,p states begins.[34] In the band gap there is an image-potential surface state that represents electrons trapped outside the surface by the image charge and kept away from the solid by Bragg reflection. Since the energy of the image state is tied to the vacuum level and since our reference level is the Fermi level, the image-state position tracks the work-function changes at the surface. For example, the image state shifts from 4.1 eV for clean Cu to 0.45-eV lower energy upon alloy formation with Mn. Our ferromagnetic first-principles calculations yield a lowering of the work function in the same energy range (0.31 eV) going from Cu(100) to $c(2\times2)$ CuMn/Cu(100). With calculations

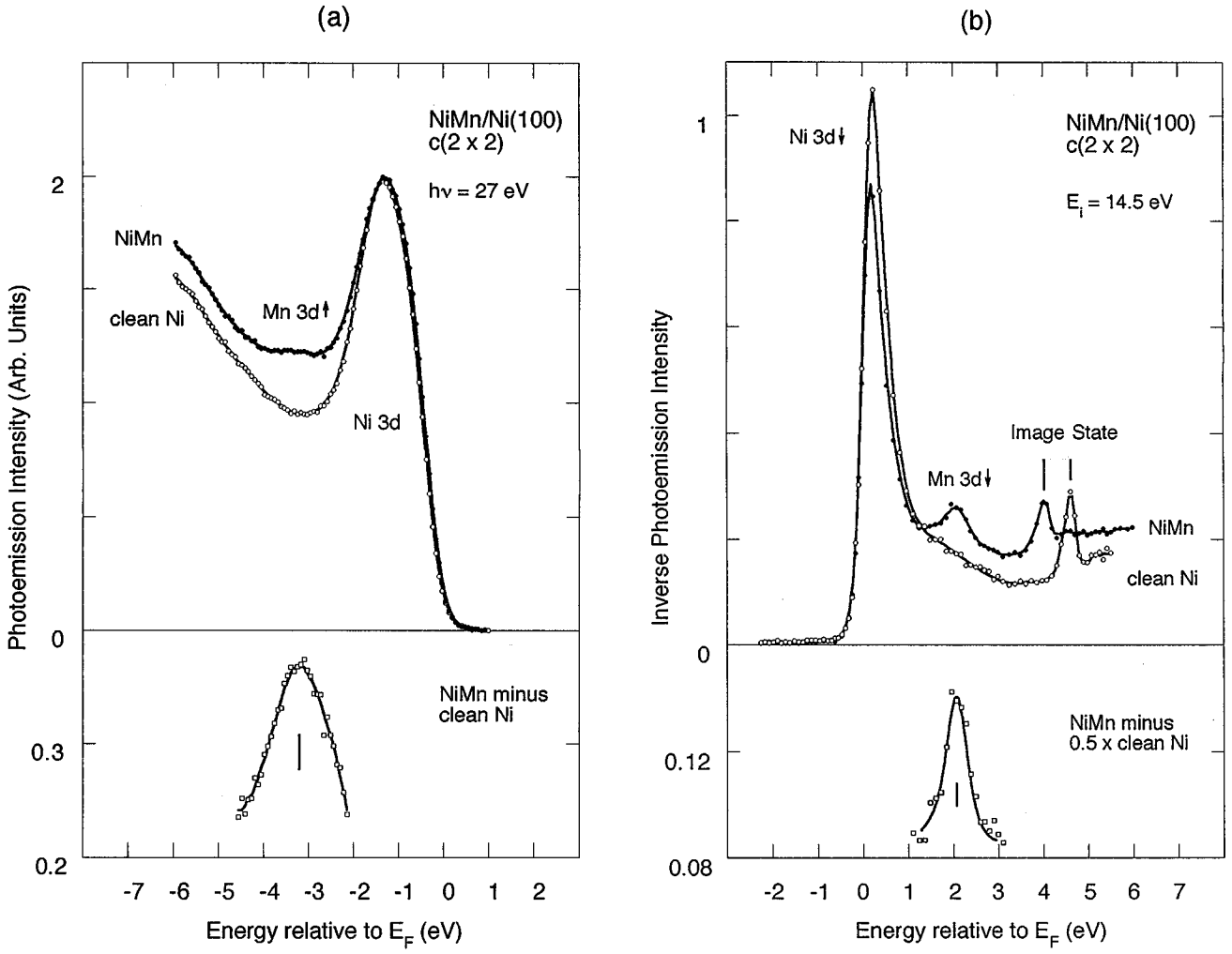

FIG. 3. Same as Fig. 2 for $c(2\times2)$ NiMn/Ni(100). Mn-3d states occur at -3.2 eV and 2.05 eV.

for a hypothetical nonmagnetic CuMn/Cu(100) surface alloy the work-function lowering amounts to only 0.05 eV. We observe further in the experiment that the image state remains about as intense as on the clean surface. The image-state emission has been found to be a sensitive indicator for the quality of the overlayer formation[11,12] and means here a very high degree of order in $c(2\times2)$ CuMn/Cu(100).

The complementary photoemission spectra of the occupied states are difficult to separate into contributions from Mn and Cu, since the clean Cu spectra are dominated by Cu-3d emission in the energy range from -2 eV to -4 eV. The spectra measured before and after Mn deposition are, in general, of a similar shape, however shifted relative to each other.[35] We have therefore selectively excited states localized at the Mn atoms by resonant photoemission. The resonant process can briefly be described as follows: For photon energies above 50 eV, the 3p excitation threshold of Mn, a Mn-3p electron can be excited into states above the Fermi level. The remaining 3p core hole can decay via a super-Coster-Kronig process giving rise to emission of a valence electron. The final state is identical to the one of direct valence-band photoemission and interferes with it. This interference leads to an enhancement of Mn-3d emission above the threshold of 50 eV. We measured spectra for photon energies between 20 eV and 59 eV,[36] and we observe at 50 eV photon energy and above it a strongly enhanced emission in the binding-energy range around the Cu-3d emission. From these spectra can readily be concluded that significant Mn-3d emission does not occur between -2 eV and the Fermi level because the spectra do not show strong emission there. The small enhancement in emission between -2 eV and E_F is probably due to a resonant enhancement of Mn s,p-derived states. A precise determination of the binding energy of Mn-3d emission from resonant photoemission spectra around 50 eV is obstructed by a strong contribution from incoherent 3p3d3d Auger emission in the valence band. We can spectroscopically separate this Auger emission from the resonant photoemission described above because the Auger peak appears at constant kinetic energy. We notice that several eV above the threshold resonant Mn photoemission is sufficiently strong so that the energy position of Mn-3d emission can be determined without Auger emission superimposed. In Fig. 2(a) we show, therefore, the resonant photoemission spectra measured at 58 eV, thus 8 eV above the threshold. Taking the difference resonance spectrum of Fig. 2(a) as a measure of the Mn contribution we find the Mn-3d majority-spin states around -3.7 ± 0.3 eV.[37]

We have also measured photoemission spectra for $c(2\times2)$

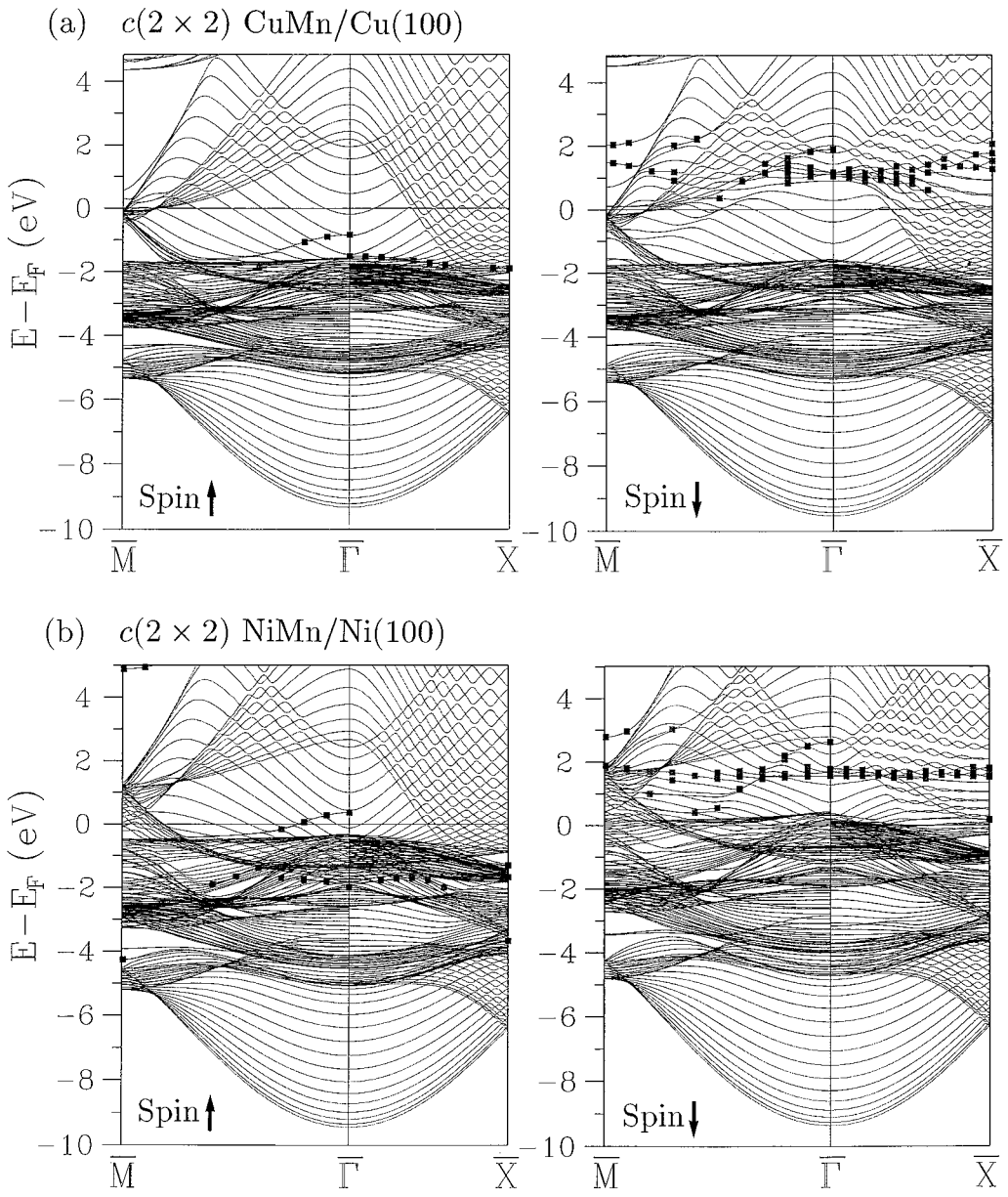

FIG. 4. (a) Two-dimensional band structure for states of even symmetry from the calculation of Fig. 1 [$c(2\times2)$ CuMn/Cu(100)]. The labels of high-symmetry points in the surface Brillouin zone are with respect to the $c(2\times2)$ superstructure. Left: Majority spin. Right: minority spin. The squares mark states the associated charge density of which is more than 60% at the Mn atoms in the surface-alloy layer. (b) Same as (a) for $c(2\times2)$ NiMn/Ni(100). Here the criterion is $>50\%$ for minority-spin states and $>30\%$ for majority spin.

NiMn/Ni(100) and clean Ni(100). As for the same structure on Cu(100) there is overlap of Mn $3d$ with substrate $3d$ states. We have measured spectra for photon energies between 20 and 45 eV. The Mn-$3d$ contribution is always present at constant energy of -3 eV but can best be extracted from the spectrum taken at 27 eV that is shown in Fig. 3(a). The broader width of the Mn emission is possibly due to the geometrical order of the superstructure, which is worse than for the Cu-based system. From the difference spectra we determine -3.2 eV as the energy position of the Mn-$3d$ states. The inverse photoemission data for $c(2\times2)$ NiMn/Ni(100) are shown in Fig. 3(b). As the Ni-$3d$ orbital is not fully occupied, it contributes a narrow peak at the Fermi level to the inverse photoemission spectrum. A Mn-$3d$ state appears at 2.05 eV above the Fermi level, which is not too far from the same state on Cu (1.85 eV). Its absolute intensity is comparable, but appears smaller in Fig. 3(b) compared to Fig. 2(b) due to a change in scale. As with $c(2\times2)$ CuMn/Cu(100) the inverse photoemission spectrum permits the conclusion that the density of states is completely spin split, so that we identify 2.05 eV with minority spin and -3.2 eV with majority spin. Also the intensity of the image state is comparable to the Cu-based system. As on Cu, a downwards shift of the image state due to lowering of the work function by Mn is observed, i.e., from 4.62–4.02 eV, which is in good agreement with our calculated work-function shift of 0.52 eV.

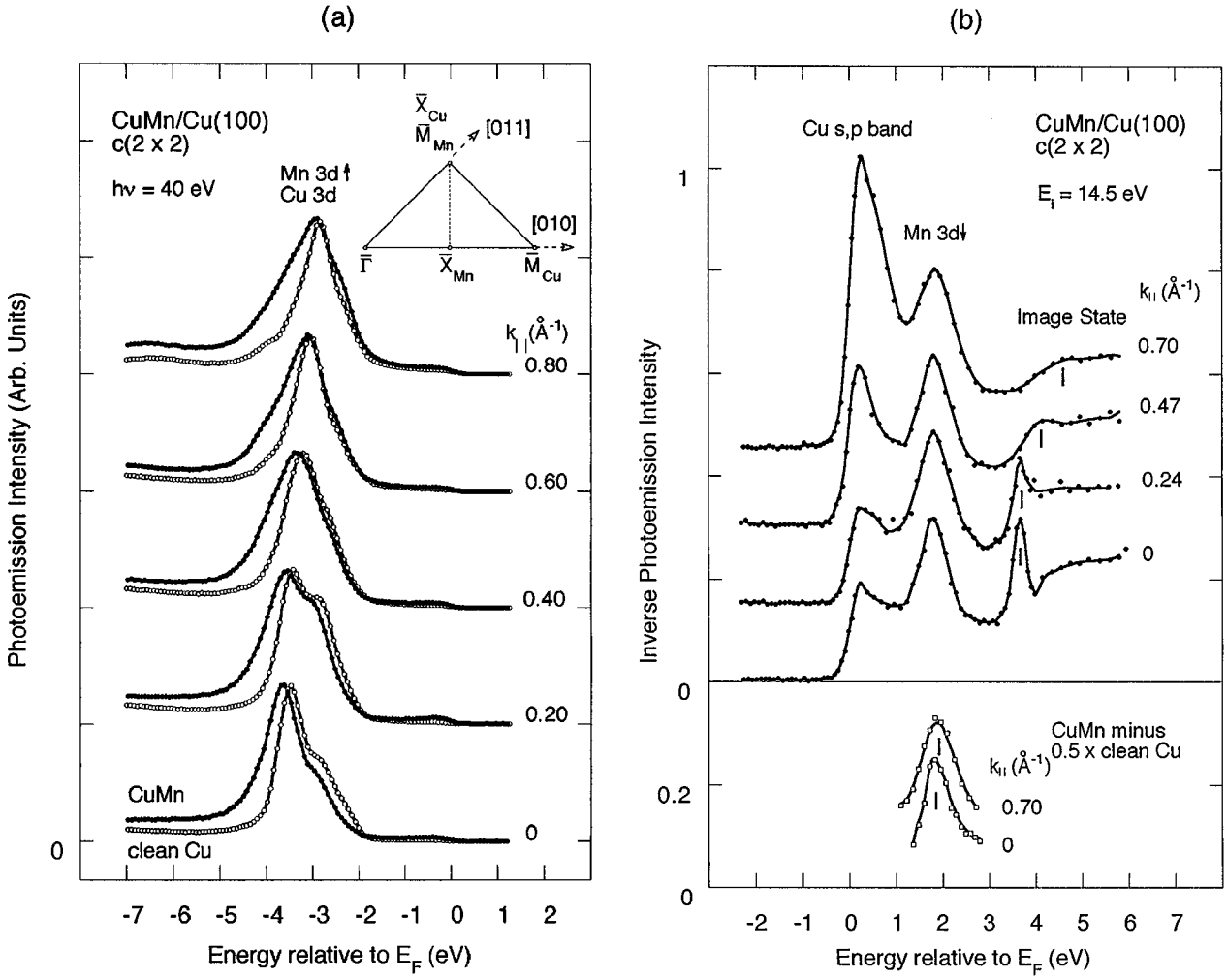

FIG. 5. Angle-resolved photoemission (a) and inverse photoemission (b) spectra for $c(2\times2)$ CuMn/Cu(100), probing the band dispersion of the Mn-3d states. A small upwards dispersion of 70 meV is found between $\mathbf{k}_{\|}=0$ and 0.70 Å^{-1}. The inset shows the Brillouin zones of the $p(1\times1)$ Cu and the $c(2\times2)$ Mn structures.

V. MAGNETIC-EXCHANGE SPLITTING

We readily obtain the magnetic-exchange splittings at the Brillouin-zone center from the majority and minority states discussed in the preceding section. We get an exchange splitting of 5.5 eV for the $c(2\times2)$ CuMn/Cu(100) system and an exchange splitting of 5.25 eV for the $c(2\times2)$ NiMn/Ni(100) system, both collected in Table I. The large splittings show directly that Mn bears a high magnetic moment in both systems. This is in agreement with a conclusion for $c(2\times2)$ CuMn/Cu(100) from absorption measurements[8] at the Mn 2p threshold. Somewhat contrasting results were found in Refs. 38 and 39. In photoemission[38] of Mn/Cu(100) it was found that Cu-3d emission is affected by Mn-Cu hybridization in agreement with our results. In addition, a virtual bound state at -1.33 eV was found[38] for low coverages (0.18–0.25 ML) Mn on Cu(100), which the authors found to be in agreement with the Mn majority-spin state at -1.44 eV calculated[40] for Mn impuries in Cu. In a photoemission study[39] of Mn on Ag(100) a prominent feature at -3.2 eV is found for low Mn coverages (0.15 ML), which grows for higher coverage and moves towards the Fermi energy (-2.7 eV at 3.5 ML).

As the present experiments were performed angle resolved, we compare them to our calculated band structure.[41] Figures 4(a) and 4(b) represent the $c(2\times2)$ CuMn/Cu(100) and $c(2\times2)$ NiMn/Ni(100) band structures in two dimensions. The left panels contain the majority-spin bands, the right panels the minority ones. For comparison with the experiment only the even-symmetry states are shown. The squares in Fig. 4 mark states localized at the Mn atom in the surface alloy layer.[42] For the $c(2\times2)$ CuMn/Cu(100) system we found for both spin-split bands two distinct Mn states at the center of the surface Brillouin-zone Γ ($\mathbf{k}_{\|}=0$): the $d_{xz,yz}$ (Γ_5 and Δ_5 in different notations) states and the ones of $d_{x^2-y^2}$d (Γ_4) symmetry, which are found to be about 0.7 eV higher in energy than the $d_{xz,yz}$ states. The exchange splitting of the states with $d_{xz,yz}$ symmetry, and only they can be measured with our experimental set-up as described in Sec. III, is then determined from the energy difference of the $d_{xz,yz}$ state in the majority-spin band at -1.55 eV and in the minority-spin band at 1.13 eV. Thus, the predicted exchange splitting at the Brillouin-zone center for the observable $d_{xz,yz}$ (Γ_5) states is 2.7 eV. For $c(2\times2)$ NiMn/Ni(100) [Fig. 4(b)] we determined the $d_{xz,yz}$ (Γ_5) minority-spin state to 1.68 eV, and its majority counterpart is found at -1.73 eV. This amounts for the $d_{xz,yz}$ states at the Brillouin-zone center to a

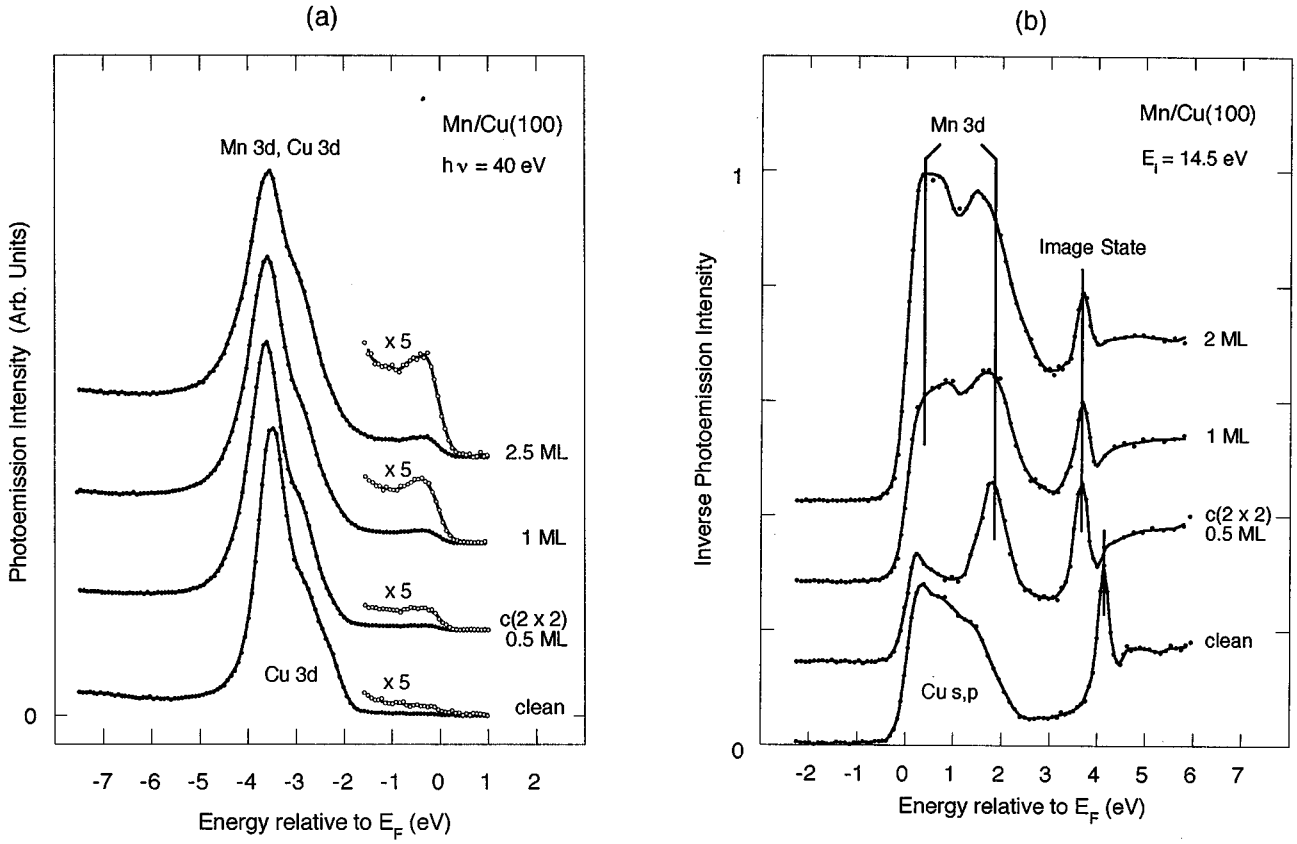

FIG. 6. Thickness dependence of photoemission (a) and inverse photoemission (b) spectra for $\mathbf{k}_{\|}=0$. As soon as the Mn amount exceeds that needed for the formation of an optimal $c(2\times2)$ superstructure, the intensity at the Fermi level increases rapidly in photoemission and inverse photoemission indicating the formation of a bulk band with small magnetic splitting. The shift of the image state shows a saturation of the work-function change at the $c(2\times2)$ structure.

predicted exchange splitting of 3.4 eV. However, the hybridization of the Mn majority states with the Ni states is stronger than with the Cu states as can be seen from Fig. 1. This mixing leads for Mn on Ni to the fact that the d_{z^2} (Γ_1) state at -1.99 eV is much stronger localized on the Mn atom than the $d_{xz,yz}$ (Γ_5) state, and the d_{z^2} state is in fact the one marked at the Brillouin-zone center in Fig. 4(b). As said in Sec. III, for NiMn the particular geometry of the photoemission experiment was such that we are sensitive to the d_{z^2} state as well, i.e., we measure a mixture of both states. With the d_{z^2} (Γ_1) minority state calculated at 1.55 eV we obtain a theoretical exchange splitting of 3.5 eV for the d_{z^2} (Γ_1) states and, as said above, of 3.4 eV for the $d_{xz,yz}$ (Γ_5) states.[43]

If we compare the experimental and theoretical values for the exchange splitting (see also Table I), we find that the experimental ones are significantly larger. The simplest argument for the reduced splitting between the majority and minority states in local-density calculations comes from the observation that local-density band theory provides eigenvalues for the neutral ground state. In an actual photoemission or inverse photoemission experiment one produces a positive and negative ion state. Therefore, an additional Coulomb energy U splits the states apart, pulling down hole states by the positive potential and electron states up by the negative potential. This effect becomes strong for increased localization of the hole and electron.[44]

Fortunately, for Mn impurities in Cu and Ag there exist experimental studies as well as first-principles local-density calculations. For Mn in Cu the calculation by Braspenning *et al.*[45] predicts the majority-spin state at about -1.7 eV and the minority state at about 0.7 eV.[46] Van der Marel *et al.*[47] saw experimentally no clear peak for the Mn majority states, but found the minority state at 1.7 ± 0.2 eV, thus about 1 eV higher than the theory. In the case of Mn in Ag, where the

TABLE I. Energy positions (in eV with respect to E_F) of spin-split Mn states in the surface alloys measured at the center of the surface Brillouin zone (Γ) are compared to eigenvalues for $d_{xz,yz}$ (Γ_5) states calculated from first principles. In addition, the calculated magnetic moments (in μ_B) are given.

	Experiment			Theory			
	$E_\uparrow$	$E_\downarrow$	ΔE	$E_\uparrow$	$E_\downarrow$	ΔE	μ
$c(2\times2)$ CuMn/Cu(100)	-3.7 ± 0.3	1.85 ± 0.1	5.5 ± 0.3	-1.55	1.13	2.68	3.75
$c(2\times2)$ NiMn/Ni(100)	-3.2 ± 0.2	2.05 ± 0.1	5.25 ± 0.2	-1.73	1.68	3.41	3.5

host d band lies deeper than in Cu, van der Marel *et al.* observe experimentally both majority and minority peaks at -3.1 ± 0.2 eV and 2.1 ± 0.2 eV, respectively. Another experiment, performed angle resolved and at higher resolution by Jordan *et al.* yields on $Ag_{85}Mn_{15}(111)$ -3.0 ± 0.1 eV (Ref. 48) and 1.7 ± 0.1 eV.[49] These experimental values for the splitting, 5.2 eV by van der Marel *et al.* and 4.7 eV by Jordan *et al.*, can be compared to the local-density calculation of Muñoz, Gyorffy, and Verhuyck[50] for Ag_xMn_{1-x} ($x=0.9$ and 0.8) that yields a splitting of 3.4 eV. An even smaller value was calculated by Podloucky, Zeller, and Dederichs.[40] However, their result of 3.02 eV is expected to increase due to a more refined calculation as did the splitting of Mn in Cu (from 2.08 eV in Ref. 40 to about 2.4 eV in Ref. 45). We conclude that the exchange/Coulomb splitting measured in photoemission and inverse photoemission from dilute Mn in Cu and Ag is almost as large as the one measured for $c(2\times2)$ CuMn/Cu(100), and that it is consistently underestimated in local-density calculations. It should be noted on the other hand that the calculated magnetic moments were, in general, found to be in agreement with the experiment.[40,45,50] This fact is consistent with the expectation that density-functional theory has a high predictive power for ground-state properties such as the local-magnetic moment, but is insufficient for properties involving electron excitations such as the exchange splitting of localized states. Comparing just the magnetic moment, our calculation gives $3.75\mu_B$ for $c(2\times2)$ CuMn/Cu(100), which is significantly larger than the value $3.4\mu_B$ calculated recently for Mn impurities in Cu.[51] For $c(2\times2)$ NiMn/Ni(100) we calculate $3.5\mu_B$ whereas the impurity calculation for Mn in Ni gives only $2.8\mu_B$.[52]

The measured splitting of Mn on Ni (5.25 eV) is smaller than the one for Mn on Cu (5.5 eV). Moreover, the ratio of measured over calculated splitting is about 1.5 on Ni and about 2 on Cu. This is believed to be due to the stronger hybridization of Mn-3d states with Ni-3d states as opposed to Cu-3d states. In the Mn local density of states of Fig. 1 the stronger effect of hybridization can be seen as a much broader Mn majority-spin density of states on Ni than on Cu. Mn-3d states are therefore expected to be less localized for Mn on Ni than for Mn on Cu. However, care must be taken in deducing the degree of Mn-substrate hybridization from the calculation. If the Mn splitting was larger in the calculation, overlap of Mn-3d with Cu-3d states would be enhanced but the Mn 3d–Ni 3d overlap would be reduced. This means the calculation might overestimate the difference between Cu and Ni substrates in terms of Mn-substrate hybridization. The fact that the difference between measured and calculated splittings is nevertheless large is in line with earlier experiments which find the behavior of Mn on Cu and Ni, in general, very similar. For example, the large outward displacement has been measured to 16.6% on Cu and 14.2% on Ni. The x-ray-absorption line shape for Mn on Cu and Ni were found identical and consistent with the spectrum calculated for a large atomiclike magnetic moment.[9]

Before closing this section we would like to mention that we performed spin-resolved photoemission for the $c(2\times2)$ CuMn/Cu(100) alloy from room temperature down to liquid-nitrogen temperature.[36] No long-range ferromagnetic order was seen in the surface plane. This extends the search for ferromagnetism in this system, initiated at room temperature with magnetic circular dichroism in Ref. 8, down to 80 K. This finding is not in contradiction to the large magnetic exchange splitting discussed above since the exchange splitting is due to the existence of large local-magnetic moments at the Mn sites. The finite-temperature properties, however, are determined by the fluctuation of the local moments.

We roughly estimated the critical temperature by adopting the Heisenberg model to describe the finite temperature properties of the $c(2\times2)$ CuMn/Cu(100) system. Following the work of Bander and Mills[53] who discussed the Heisenberg model with a single ion anisotropy, the critical temperature of an ultrathin film is proportional to the interatomic exchange integral J,[54] which may be estimated from the total energy that is involved in the magnetic ordering of a Mn monolayer on Cu(100) and the $c(2\times2)$ CuMn/Cu(100) surface alloy. $J=(E_{\text{ferro}}-E_{\text{antiferro}})/2M^2$ is then calculated from the energy difference of the total energies for ferromagnetic (E_{ferro}) and antiferromagnetic ($E_{\text{antiferro}}$) coupling and the calculated magnetic moment M.[55] In this way we estimate $J_{\text{surface alloy}}$ comparing the $c(2\times2)$ ferromagnetic structure with the $p(2\times2)$ antiferromagnetic superstructure of the $c(2\times2)$ surface alloy. As a reference value we also calculate $J_{\text{monolayer}}$ for a complete $p(1\times1)$ monolayer Mn/Cu(100) comparing the total energies of the $p(1\times1)$ ferromagnetic structure with the $c(2\times2)$ antiferromagnetic structure. We find a ratio for the exchange integrals of $J_{\text{surface alloy}}/J_{\text{monolayer}}\approx\frac{1}{6}$. If we assume a critical temperature for the monolayer on Cu(100) around room temperature, which is typical for monolayer systems,[56] we estimate the critical temperature for the surface alloy to be less than 50 K. Furthermore, we found that the $p(2\times2)$ antiferromagnetic phase is higher in energy than the $c(2\times2)$ ferromagnetic one and very likely the ground state of the surface alloy may indeed be ferromagnetic. The $c(2\times2)$ NiMn/Ni(100) surface alloy, on the other hand, is from the thermodynamical point of view a semi-infinite system, and the critical temperature of the surface alloy has been found to be the critical temperature of the Ni substrate.[10]

VI. BAND DISPERSION

We want to estimate the degree of localization of the Mn-3d states in the $c(2\times2)$ CuMn/Cu(100) alloy from the bandwidth. Therefore, we have traced the dispersion of the observed Mn structures with the wave vector parallel to the surface $\mathbf{k}_\parallel$ in photoemission and inverse photoemission. Figure 5(b) shows the inverse photoemission spectra; where the Mn-3d peak can be followed without 3d contribution from Cu, for $\mathbf{k}_\parallel=0$, 0.24, 0.47, and 0.70 Å^{-1}. The sample was turned in the $\Gamma M_{\text{Mn}}=\Gamma X_{\text{Cu}}$ direction with $M_{\text{Mn}}=X_{\text{Cu}}=1.23$ Å^{-1}. A small upwards dispersion of 70 ± 40 meV from $\mathbf{k}_\parallel=0$ (1.85 eV) to 0.70 Å^{-1} (1.92 eV) is obtained. The measurement 0.70 Å^{-1} corresponds to about half of the Brillouin-zone edge of the $c(2\times2)$ structure. Approximating the Mn-3d band dispersion by a cosine function, we can infer the width of this band as 110 ± 60 meV or, alternatively, the effective mass at Γ as $m^*=20m_e$. These values indicate a high localization of the Mn-3d minority states. It can be understood as due to the geometrical separation of the Mn

atoms and the weak overlap of Mn-3d orbitals. The image-potential state, in contrast, disperses strongly from 3.67 eV ($\mathbf{k}_{\|}=0$) to 4.60 eV ($\mathbf{k}_{\|}=0.70$ Å^{-1}), corresponding to its free-electron-like nature in two dimensions.

We can compare the measured dispersion of the Mn-3d minority state with the calculated one from Fig. 4(a). Subtracting the energy of the $d_{xz,yz}$ (Γ_5) state from the corresponding state at M_{Mn} gives a small value for the bandwidth of approximately 0.2 eV.

The angle-dependent photoemission spectra are shown in Fig. 5(a). The sample was turned in the ΓX_{Mn} direction. A clearcut dispersion of the majority Mn states as predicted in Fig. 4(a) is not observed. This is not surprising as the calculation predicts the Mn-3d states at energy positions well separated from the ones of Cu-3d states and may therefore also underestimate the mixing between both.

VII. COLLAPSE OF THE MAGNETIC SPLITTING TOWARDS BULK Mn

The spectra in Fig. 6 show what happens if the nominal Mn coverage on Cu(100) is increased beyond the 0.5 ML that are needed to form the $c(2\times2)$ structure. The photoemission spectra of Fig. 6(a) show that the second 0.5 ML added after the $c(2\times2)$ has attained optimum quality in the LEED leads to an increase in emission in the vicinity of the Fermi energy. At 2.5 ML this emission continues to grow. This was also observed on the same system in Ref. 38 and on Mn on Ag(100) in Ref. 39 despite the different interpretation in Ref. 39.

Corresponding emission at the Fermi level appears in the inverse photoemission spectra in Fig. 6(b). Here it is further seen that the Mn-3d intensity at the Fermi level grows in the first instance leaving the 3d minority peak at 1.85 eV intact. When increasing the nominal coverage to 2 ML the emission at the Fermi level predominates. This was also observed for Mn on Ag(111) (Ref. 33) and Ag(100).[11]

This means that, as soon as the Mn-Mn coordination is increased beyond the $c(2\times2)$, the magnetic exchange splitting collapses. Excess Mn atoms that are built in lead to a transfer of spectral weight towards the Fermi level and are therefore considered to be nonferromagnetic. The calculated density of states for a complete monolayer Mn/Cu(100) (not shown), for which antiferromagnetic order with the opposite spins occupying the sites of a checkerboard has lowest total energy, predicts high intensity around the Fermi level. In conclusion, the large exchange splitting and consequently the high magnetic moment are exclusively a property of the $c(2\times2)$ surface alloy.

VIII. SUMMARY

Angle-resolved photoemission and inverse photoemission spectra of $c(2\times2)$ CuMn/Cu(100) and $c(2\times2)$ NiMn/Ni(100) have been measured. The results were compared to our first-principles calculations for $c(2\times2)$ CuMn/Cu(100) and $c(2\times2)$ NiMn/Ni(100), which exhibit large magnetic moments for Mn, $3.75\mu_B$ for the $c(2\times2)$ CuMn/Cu(100) alloy and $3.5\mu_B$ for the $c(2\times2)$ NiMn/Ni(100) alloy. The measured exchange/Coulomb splittings at the Brillouin-zone center are large (5.5 eV for the Cu-based system and 5.25 eV for the Ni-based system), which proves that the Mn bears a high magnetic moment in these systems. From first principles we calculate exchange splittings of 2.7 eV for $c(2\times2)$ CuMn/Cu(100) and 3.5 eV for $c(2\times2)$ NiMn/Ni(100), thus significantly smaller than measured. We suppose that this difference is due to an additional Coulomb energy U, which splits the final states in photoemission and inverse photoemission apart. This effect requires a high localization of the Mn states that we indeed observe in the small measured and calculated band dispersion for $c(2\times2)$ CuMn/Cu(100). The Mn-thickness-dependent spectra on Cu show that the splitting collapses for coverages above the half monolayer needed to form the $c(2\times2)$ superstructure. Comparison with the systems Fe/Au(100) and Cr/Ag(100) does not indicate large discrepancies between measured splittings and the local-density description as we observe them for the dilute half-monolayer system. This means a qualitatively different electronic structure due to extra localization in 0.5 ML versus 1 ML. In spite of a larger expected hybridization of Mn-3d states with the Ni substrate we find a similar behavior for Mn on Ni. We also investigated the work-function change upon the formation of surface alloys. We found a very nice agreement between theory and experiment. A comparison of ferromagnetic CuMn/Cu(100) with hypothetical nonmagnetic CuMn/Cu(100) identified the formation of high magnetic moments as the basic origin of the large modification of the electronic structure that causes the work-function change.

Note added. We recently noticed the publication of Hayden, Pervan, and Woodruff (Ref. 57). We find the reported inverse-photoemission spectra of $c(2\times2)$ CuMn/Cu(100) and of thicker Mn/Cu(100) in good agreement with our results.

ACKNOWLEDGMENTS

O.R. acknowledges financial support by Verein der Freunde und Förderer von BESSY e. V and the support of IBM Thomas J. Watson Research Center. We thank Professor A. Fujimori for helpful discussions. Computations were performed on Cray computers of Forschungszentrum Jülich and the German supercomputer center (HLRZ).

*Present address: Department of Physics, University of Tokyo, 7-3-1 Hongo, Bunkyo-ku, Tokyo 113, Japan. Electronic address: rader@exp.bessy.de

†Present address: National Synchrotron Light Source, National Laboratory, Upton, NY 11973.

‡Present address: Department of Physics, University of Wisconsin Madison, 1150 University Ave., Madison, WI 53706.

[1] T. Flores, M. Hansen, and M. Wuttig, Surf. Sci. **279**, 251 (1992).

[2] M. Wuttig, Y. Gauthier, and S. Blügel, Phys. Rev. Lett. **70**, 3619 (1993).

[3] M. Wuttig, T. Flores, and C. C. Knight, Phys. Rev. B **48**, 12 082 (1993).

[4] M. Wuttig, C. C. Knight, T. Flores, and Y. Gauthier, Surf. Sci. **292**, 189 (1993).

[5] Z. Q. Wang, Y. S. Li, C. K. C. Lok, J. Quinn, F. Jona, and P. M. Marcus, Solid State Commun. **62**, 181 (1987).

[6] S. C. Wu, S. H. Lu, Z. Q. Wang, C. K. C. Lok, J. Quinn, Y. S. Li, D. Tian, F. Jona, and P. M. Marcus, Phys. Rev. B **38**, 5363 (1988).
[7] S. Blügel (unpublished).
[8] W. L. O'Brien, J. Zhang, and B. P. Tonner, J. Phys. Condens. Matter **5**, L515 (1993); W. L. O'Brien and B. P. Tonner, J. Appl. Phys. **76**, 6468 (1994).
[9] W. L. O'Brien and B. P. Tonner, Phys. Rev. B **51**, 617 (1995).
[10] D. Schmitz, O. Rader, C. Carbone, and W. Eberhardt, Phys. Rev. B **54**, 15 352 (1996).
[11] J. E. Ortega and F. J. Himpsel, Phys. Rev. B **47**, 16 441 (1993).
[12] M. E. Haugan, Qibiao Chen, M. Onellion, and F. J. Himpsel, Phys. Rev. B **49**, 14 028 (1994).
[13] W. Heinen, C. Carbone, T. Kachel, and W. Gudat, J. Electron Spectrosc. Relat. Phenom. **51**, 701 (1990).
[14] F. J. Himpsel, Phys. Rev. B **44**, 5966 (1991).
[15] C. L. Fu, A. J. Freeman, and T. Oguchi, Phys. Rev. Lett. **54**, 2700 (1985); Chun Li, A. J. Freeman, and C. L. Fu, J. Magn. Magn. Mater. **75**, 201 (1988); Chun Li, A. J. Freeman, H. J. F. Jansen, and C. L. Fu, Phys. Rev. B **42**, 5433 (1990).
[16] C. Krembel, M. C. Hanf, J. C. Peruchetti, D. Bolmont, and G. Gewinner, Phys. Rev. B **44**, 11 472 (1991).
[17] S. Blügel, M. Weinert, and P. H. Dederichs, Phys. Rev. Lett. **60**, 1077 (1988); S. Blügel, B. Drittler, R. Zeller, and P. H. Dederichs, Appl. Phys. A **49**, 547 (1989); S. Blügel, Phys. Rev. Lett. **68**, 851 (1992).
[18] A. Santoni and F. J. Himpsel, Phys. Rev. B **43**, 1305 (1991).
[19] L. W. Bos and D. W. Lynch, Phys. Rev. B **2**, 4567 (1970).
[20] J. R. Davis and T. J. Hicks, J. Phys. F **9**, 753 (1979).
[21] R. J. Higgins and R. H. Hendel, Solid State Commun. **39**, 47 (1981).
[22] J. W. Cable and H. R. Child, Phys. Rev. B **10**, 4607 (1974).
[23] T. Böske, W. Clemens, C. Carbone, and W. Eberhardt, Phys. Rev. B **49**, 4003 (1994).
[24] U. von Barth and L. Hedin, J. Phys. C **5**, 1629 (1972); V. L. Moruzzi, J. F. Janak, and A. R. Williams, *Calculated Electronic Properties of Metals* (Pergamon, New York, 1978).
[25] E. Wimmer, H. Krakauer, M. Weinert, and A. J. Freeman, Phys. Rev. B **24**, 864 (1981); M. Weinert, E. Wimmer, and A. J. Freeman, *ibid.* **26**, 4571 (1982).
[26] We show results with a structural configuration $\Delta z_{\mathrm{Cu}}=-2\%$; $\Delta z_{\mathrm{Mn}}=+11\%$ for the CuMn alloy and $\Delta z_{\mathrm{Ni}}=-2\%$; $\Delta z_{\mathrm{Mn}}=+8\%$ for the NiMn alloy, which are close to the structural optimum determined by energy minimization. The origin of Δz are the atom positions of the ideal bulk-truncated Cu(100) [Ni(100)] surface.
[27] A. Clarke, N. B. Brookes, P. D. Johnson, M. Weinert, B. Sincovic, and N. V. Smith, Phys. Rev. B **41**, 9659 (1990).
[28] Th. Fauster, D. Straub, J. J. Donelon, D. Grimm, A. Marx, and F. J. Himpsel, Rev. Sci. Instrum. **56**, 1212 (1985).
[29] E. Kisker and C. Carbone, in *Angle Resolved Photoemission*, edited by S. D. Kevan (Elsevier, Amsterdam, 1992).
[30] W. Gudat, E. Kisker, G. M. Rothberg, and C. Depautex, Nucl. Instrum. Methods **195**, 233 (1982).
[31] M. H. Mohamed, J.-S. Kim, and L. L. Kesmodel, Phys. Rev. B **40**, 1305 (1985); Y. Chen, S. Y. Tong, J.-S. Kim, M. H. Mohamed, and L. L. Kesmodel, Phys. Rev. B **43**, 6788 (1991); J.-S. Kim, M. H. Mohamed, and L. L. Kesmodel, Surf. Sci. **260**, 185 (1992).
[32] B. Schulz, R. Schwarzwald, and K. Baberschke, Surf. Sci. **307-309**, 1102 (1994).
[33] W. Drube and F. J. Himpsel, Phys. Rev. B **35**, 4131 (1987).
[34] F. J. Himpsel and J. E. Ortega, Phys. Rev. B **46**, 9719 (1992).
[35] Spectra taken at 40 eV photon energy are displayed in Figs. 5(a) and 6(a).
[36] O. Rader, Ph.D. thesis, Freie Universität Berlin, 1994.
[37] The error margin of ± 0.3 eV accounts for uncertainties in the intensity normalization, which was done on the basis of the photocurrent measured from the sample.
[38] C. Binns and C. Norris, Surf. Sci. **116**, 338 (1982).
[39] D. A. Newstead, C. Norris, C. Binns, A. D. Johnson, and M.-G. Barthès, J. Phys. C **21**, 3777 (1988).
[40] R. Podloucky, R. Zeller, and P. H. Dederichs, Phys. Rev. B **22**, 5777 (1980).
[41] Although the resonant process contributing to the photoemission at 58 eV does not necessarily conserve the wave vector parallel to the surface $\mathbf{k}_{\parallel}$, a comparison with the $\bar{\Gamma}$ point is justified by the small dispersion as revealed in Sec. VI.
[42] Mn states are identified as states that lead to a concentration of their charge density in muffin-tin spheres of the Mn. The criterion is >60% charge density at the Mn for $c(2\times2)$ CuMn/Cu(100) and >50% for minority-spin states of $c(2\times2)$ NiMn/Ni(100) and >30% for majority. This distinction is necessary because the spin-dependent Mn-3d–substrate-3d hybridization affects the majority states much more than the minority states.
[43] In the NiMn surface alloy the calculated exchange splittings of Mn-3d states vary with the orbital symmetry and the location in the surface Brillouin zone. For example, $\underline{d_{x^2-y^2}}$ ($\bar{\Gamma}_4$) states in NiMn are by 1 eV less split than $d_{xz,yz}$ ($\bar{\Gamma}_5$) states. In contrast, for the CuMn surface alloy the influence of the substrate is weaker and the dependence of the exchange splitting on the orbital symmetry is much smaller. The exchange splitting of $d_{x^2-y^2}$ ($\bar{\Gamma}_4$) states is here about the same as of the $d_{xz,yz}$ ($\bar{\Gamma}_5$) states.
[44] From Table I we further notice that the energy positions from measurement and local-density calculation agree better for the unoccupied states than for the occupied states. This observation has already been made for transition-metal oxides and is ascribed to the self-interaction problem in local-density theory. For photoemission spectra this has been discussed earlier [A. Fujimori and F. Minami, Phys. Rev. B **30**, 957 (1984); G. A. Sawatzky and J. W. Allen, Phys. Rev. Lett. **53**, 2339 (1984)].
[45] P. J. Braspenning, R. Zeller, A. Lodder, and P. H. Dederichs, Phys. Rev. B **29**, 703 (1984).
[46] Values inferred from a figure in Ref. 45.
[47] D. van der Marel, C. Westra, G. A. Sawatzky, and F. U. Hillebrecht, Phys. Rev. B **31**, 1936 (1985); D. van der Marel, G. A. Sawatzky, and F. U. Hillebrecht, Phys. Rev. Lett. **53**, 206 (1984).
[48] R. G. Jordan and G. S. Sohal, J. Phys. C **16**, L529 (1983); R. G. Jordan, Vacuum **33**, 827 (1983).
[49] R. G. Jordan, W. Drube, D. Straub, and F. J. Himpsel, Phys. Rev. B **33**, 5280 (1986).
[50] M. C. Muñoz, B. L. Gyorffy, and K. Verhuyck, J. Phys. F **13**, 1847 (1983).
[51] N. Papanikolaou, N. Stefanou, R. Zeller, and P. H. Dederichs, Phys. Rev. B **46**, 10 858 (1992).

[52] S. Blügel, H. Akai, R. Zeller, and P. H. Dederichs, Phys. Rev. B **35**, 3271 (1987).

[53] M. Bander and D. L. Mills, Phys. Rev. B **38**, 12 015 (1988).

[54] The interatomic exchange J should not be confused with the intraatomic exchange of Mn, responsible for the large magnetic moments of Mn.

[55] We verified that the magnetic moment does not change significantly between ferromagnetic and $p(2\times2)$ antiferromagnetic coupling. Using the same enlarged unit cell and a reduced number of **k** points, we obtain $M_{\text{antiferro}}=3.73\mu_B$ and $M_{\text{ferro}}=3.64\mu_B$.

[56] W. Dürr, M. Taborelli, O. Paul, R. Germar, W. Gudat, D. Pescia, and M. Landolt, Phys. Rev. Lett. **62**, 1206 (1989).

[57] A. B. Hayden, P. Pervan, and D. P. Woodruff, J. Phys. Condens. Matter **7**, 1139 (1995).